Radio Science, Volume 21, Number 1, Pages 25–46, January–February 1986

Measurement and statistical analysis of wideband MF atmospheric radio noise 1. Structure and distribution and time variation of noise power

J. R. Herman,[1] *A. A. Giordano,*[2,3] *X. A. DeAngelis,*[1]
K. F. Marzotto,[2] *and F. M. Hsu*[2]

(Received July 2, 1985; accepted August 2, 1985.)

Wideband measurements (100 kHz) of medium frequency atmospheric noise have been made over the past several years in the southwestern United States. In part 1 of a two-part paper the measurement and data transcription system and the statistical analysis software used to analyze the data are presented. In part 2, representative first- and higher-order statistics and the impact of the data on bandwidth and system performance are described. Measurement results presented in part 1 include the temporal structure of atmospheric noise, the distribution and time variation of the measured average noise power, and comparisons with predictions by the International Radio Consultative Committee (CCIR).

1. INTRODUCTION

Recent developments in the use of spread spectrum techniques in communications systems have led to an interest in the properties of wideband atmospheric radio noise and its effects on system performance. Inasmuch as most noise data bases, simulation models, and prediction models [e.g., *International Radio Consultative Committee* (*CCIR*), 1964] are derived from narrow band measurements, extrapolation to wideband applications may be misleading. It is thus desirable to ascertain wideband noise characteristics through direct measurement. An experimental program was carried out to do this for a portion of the medium frequency (MF) band. The program employed a unique noise-measuring and -recording system to collect wideband atmospheric noise data and analysis software to extract first- and higher-order noise statistics. The work reported here is a comprehensive extension of earlier preliminary work by *Sunkenberg et al.* [1980]; *Marzotto et al.* [1982], and *Herman et al.* [1983].

The results of this effort are presented in two parts. Part 1 describes the measurement, transcription, and data analysis system and provides comparisons of seasonal and diurnal measurements of average noise power with CCIR predictions. Part 2 presents first- and higher-order statistics determined from the measured noise and compares simulated performance of nonlinear receivers operating in measured and modeled atmospheric noise.

Noise parameters of interest include the impulsiveness of the noise, as indicated by the voltage deviation V_d, defined as the ratio (decibels) of rms to average noise envelope voltage, the amplitude probability distribution (APD), the average crossing rate (ACR), and the effective antenna noise factor F_a, which represents the external noise power available from a loss-free antenna. In addition to these first-order statistics of potential interest, several higher-order noise statistics include the pulse spacing distribution (PSD), the pulse duration distribution (PDD), the autocorrelation function (ACF), and the power density spectrum (PDS).

To obtain these characteristics and their variations with time, field measurements and recordings were made in a rural location near Tonapah, Nevada, six times per day in time blocks, as defined by *CCIR* [1964], during three seasonal periods: September 7 to October 6, 1980; February 16 to March 16, 1980; and July 14 to August 22, 1981. The instrumentation and antennas, described more fully in section 2, consisted of two separate equipment systems, referred to here as an "atmospheric noise recording (ANR) system" and an "APD monitor." Each system could be connected to either or both of the antennas (a vertical dipole, and a horizontal crossed dipole). In

[1]Strategic Systems Division, GTE Government Systems Corporation, Westborough, Massachusetts.
[2]Communications Systems Division, GTE Government Systems Corporation, Needham Heights, Massachusetts.
[3]Now at CNR, Incorporated, Needham, Massachusetts.

Paper number 5S0624.
0048-6604/86/005S-0624$08.00

TABLE 1. Distribution of Noise Recordings by Time

	Number of 5-min Digital Tape Recordings		
	Fall	Winter	Summer
	September 7 to October 6, 1980	February 16 to March 16, 1981	July 14 to August 22, 1981
Time block, hours			
00–400	22	29	55
400–800	22	30	38
800–1200	22	29	36
1200–1600	27	35	43
1600–2000	29	33	39
2000–2400	27	30	41
Total recordings	149	186	252

normal field operations each noise-recording sequence was preceded by a sampling of the noise from each antenna by the APD monitor, whose manually recorded output provided quick estimates of the current APD, V_d, and noise power needed to establish the required gain and dynamic range settings of the noise-recording system. During the winter and summer measurement periods the noise from one antenna was again sampled by the APD monitor immediately after each recording. The ANR system recorded approximately 5-min samples of the ambient wideband noise (100-kHz bandwidth centered nominally at 450 kHz) from each antenna, either sequentially or simultaneously using multiplexing, on high-density data tapes. The total number of recordings by time block and season are noted in Table 1.

For computer processing the high-density field tapes were transcribed to computer compatible magnetic tapes following the procedures outlined in section 3. The transcriptions were then analyzed using the software described in section 4. Digital band-pass filtering allowed investigation of bandwidth effects, and digital notch filters were used to excise interfering carriers. In section 5 the temporal structure of atmospheric noise and the distribution and time variation of the measured average noise power (expressed as F_a) are presented. Diurnal and seasonal variations of the noise power factor are then compared with *CCIR* [1964] predictions.

In part 2 of this effort, first-order statistics of wideband MF atmospheric noise, such as the APD and higher-order statistics, for example, the PSD, PDD, ACF, etc., are presented. Subsequently, bit error rate simulations of coherent receivers operating in measured and modeled atmospheric noise environments are obtained.

2. NOISE MEASUREMENT SYSTEM

The noise measurement system is an enhanced version of the system used in prior noise measurements and reported previously [*Sunkenberg et al.*, 1980]. The system consists of three major elements: (1) data-collection hardware and field operations, (2) transcription equipment and software to convert the field data to a computer compatible format, and (3) computer software for data processing and analysis. Each element is described below.

The principal features of the earlier system were maintained in the current version. These features permit recording of wideband MF noise measurements on a high-speed digital tape recorder system for subsequent data analysis. Data can be recorded at several center frequencies with a bandwidth as wide as 100 kHz. Log compression and decompression yield a system dynamic range of approximately 120 dB. The current noise measurement system includes an expanded capability for simultaneous dual-channel recordings. The dual-channel capability permits measurements with different polarizations and antenna configurations. Another significant enhancement is provided with the addition of a continuous encode/decode/deskewing system which substantially reduces errors introduced on the high-density digital tape recordings. Further improvements to the noise measurement system, which have recently been completed, permit HF channel recordings and real-time playback for testing laboratory receivers.

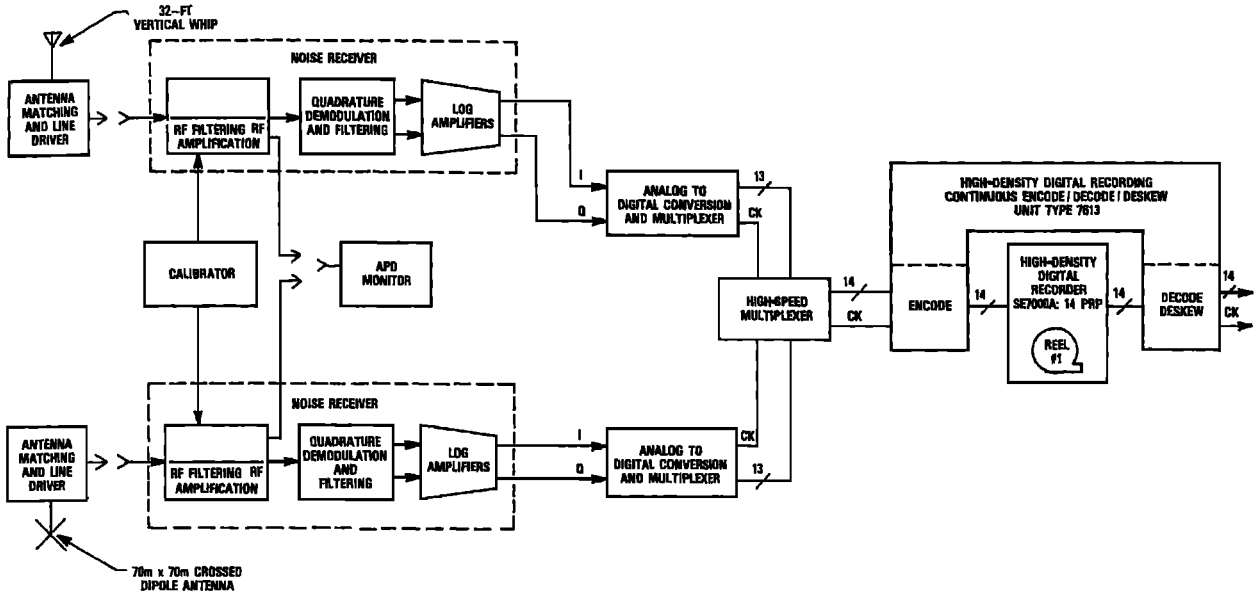

Fig. 1. Noise-recording system.

TABLE 2. System Parameters, Summer 1981 Measurement Period

Parameter	Identification
Center frequencies	380 kHz, 412.5 kHz, 437.5 kHz, 450 kHz, 462.5 kHz, 487.5 kHz
Receiver bandwidths	25 kHz, 50 kHz, 100 kHz
Duration of recording	in each 4-hour time block over 24 hours, one 1.5-min data run (simultaneous) from vertical whip and normal cross-dipole antennas one 1-min data run (simultaneous) from normal quadrature outputs of cross-dipole antennas two 5-min data runs (sequential) from vertical whip and normal crossed-dipole antennas
Sampling rate	255 kHz (complex from each antenna)
Number of samples in each data run	4.6×10^7 from each antenna in 1.5-min simultaneous run 3.1×10^7 from each antenna in 1-min simultaneous run 1.5×10^8 in each 5-min sequential run
Measurement period	July 15, 1981, through August 22, 1981
Site	Stone Cabin Valley, Nevada
Antenna types	10 m vertical 70 × 70 m crossed-dipole, three element, normal and quadrature outputs

2.1. *Noise-recording subsystem*

A functional block diagram of the noise measurement system and associated system parameters permitted during the summer 1981 measurement period are shown in Figure 1 and Table 2, respectively. In Figure 1 it can be seen that both analog and digital processing is used to generate the high-density digital noise recordings. Two antennas, described in more detail below, were used in the noise measurements. The antenna configurations include a vertical whip and a lightly buried horizontal crossed dipole with right-hand circular (RHC) and left-hand circular (LHC) polarization outputs. An antenna-matching network and a line driver are provided for each antenna. A set of band-pass filters allows selection of an MF carrier frequency and a receiver bandwidth of up to 100 kHz (see Table 2). Following RF filtering, the noise is amplified and heterodyned to base band, using quadrature demodulation. To accommodate the wide dynamic range of the atmospheric noise, two variable-gain, matched bipolar logarithmic amplifiers are used. These amplifiers operate with a nominal 0.33 logarithmic compression factor, so that an input dynamic range of 120 dB will be limited to an output range of 40 dB. The logarithmic amplifier outputs feed a pair of sample and hold circuits which

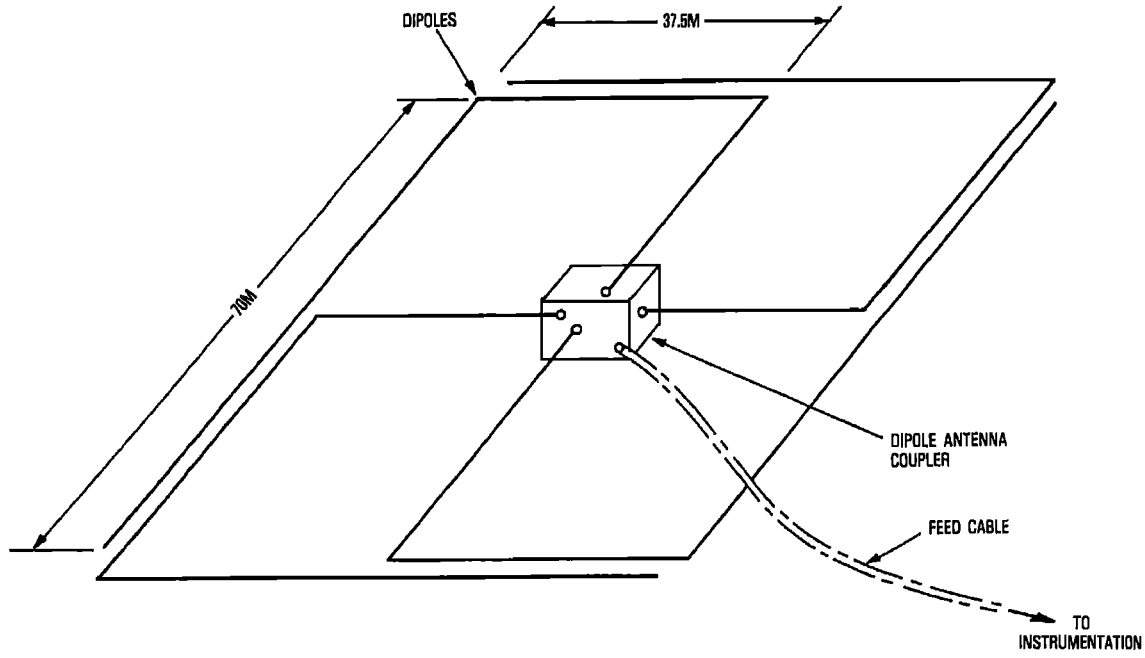

Fig. 2. Buried insulated wire, dipole array antenna configuration.

sample the inphase and quadrature channel simultaneously at a 255-kHz rate. The two 12-bit parallel 255-kHz signals from the quadrature channel analog to digital (A/D) converters are time division multiplexed along with a channel select signal from the multiplexing operation and a parity bit on the 12 data bits. As a result, a 14-bit parallel 510-kHz data stream is produced. Further multiplexing (Figure 1) allows simultaneous recording from both antennas. The multiplexed digitized signal stream is recorded on high-density digital tape by use of an encode/decode/deskew unit. This unit accepts the digitized signal from the multiplexer, encodes it for storage on the 14-track digital recorder and decodes and deskews it on playback for subsequent transcription. As a result, tape errors introduced during recording are significantly reduced. Using this procedure, up to 5-min data runs are made in each 4-hour time block over a 24-hour period (see Table 2).

2.2. *Antenna subsystem*

The vertical whip used in the measurements is 10 m in height. This antenna has an effective height of 4.9 m, independent of the MF carrier frequency selected. The RF sensitivity obtained with this antenna results in a noise figure of 31 dB relative to thermal noise.

The horizontal crossed-dipole antenna is 70 by 70 m and has approximately an omnidirectional pattern. A sketch of the dipole array, shown in Figure 2 depicts the dual-feed cables for RHC and LHC outputs. Feeding the individual crossed-dipole signals to a quadrature hybrid permits the antenna to be responsive to either right-hand circular or left-hand circular skywave polarization. Both polarizations yield an omnidirectional ground wave pattern. Since both polarizations will yield the same response to a vertically polarized ground wave, polarization data can be taken which, on a short-term basis, indicates when the noise is dominated by left- or right-hand circular polarization. These results can be useful in a polarization diversity system where superior system performance is attained from using the channel with lower noise.

It should be noted that the vertical antenna responds only to the vertical electric field component, while the crossed dipole responds to both vertical and horizontal components of the field. As a result, data on the magnitude and phase relationships among these components are then made available by the use of simultaneous measurements.

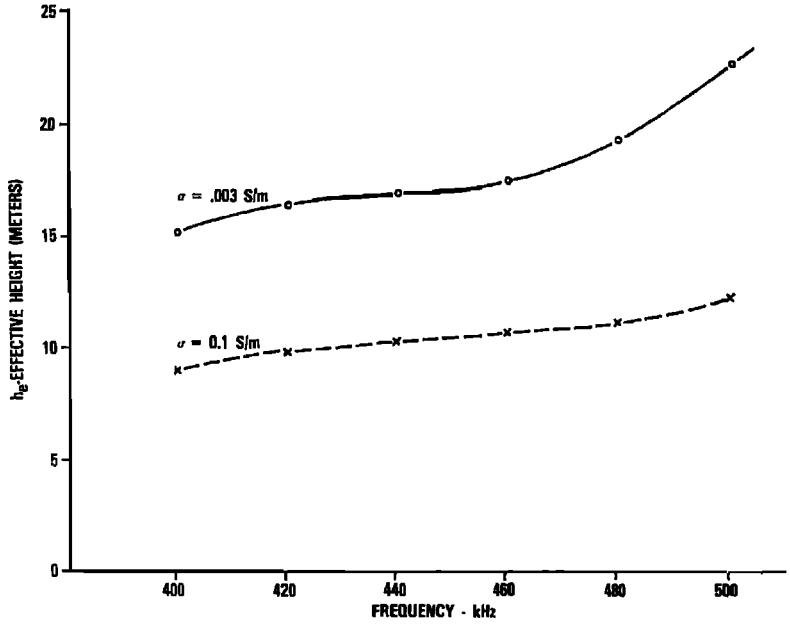

Fig. 3. Effective height of dipole array for space wave field component at beam peak as a function of frequency.

The theoretical effective height of the crossed-dipole antenna varies with soil conductivity and frequency, as shown in Figure 3. To determine the effective height of the crossed-dipole antenna for vertical polarization at the field site, measurements were made. The calibrations were accomplished by transmitting a low-level, vertically polarized signal from a test antenna and measuring the received signals on the vertical whip and crossed-dipole antennas. Measurements were made at five frequencies spaced across the 400- to 500-kHz band from each of nine transmitter sites. Average values of the effective height of the crossed-dipole antenna configurations corresponding to the normal and quadrature outputs are 12.1 and 14.4 m, respectively. Prior winter measurements made for the normal output had resulted in a 6.33-m effective height. This difference may be attributed to unusually high ground conductivity during the winter months caused by almost daily snowfalls and subsequent melting, which resulted in water-saturated soil conditions.

2.3. *System performance*

In order to measure accurately the atmospheric noise environment at MF, the average received noise level in a 1-Hz band relative to the thermal noise must exceed the receiving system operating noise figure, as defined by *CCIR* [1964, 1966]. The 0-dB received "signal"-to-noise ratio (SNR) condition occurs when the received atmospheric noise level ("signal") is just equal to the receiving system operating noise figure. In order to measure the wideband atmospheric noise properties a received SNR of 10 dB or better is required. A comparison of the receiver noise figure with the expected range of received atmospheric noise level from *CCIR* [1964] indicates that the received average SNR is between 15 and 54 dB for the spring, winter, and summer periods, thereby assuring good measurement accuracy.

An analysis was performed to examine the impact on SNR of 12-bit A/D conversion, log compression, and inverse log compression. The resulting average SNR was determined to be in excess of 56 dB, so that the 31-dB receiver sensitivity establishes the minimum noise level for the measurement system.

The system linearity was measured from the antenna output to the output of the software-implemented inverse log compression. The results indicate that the degradation from system linearity is less than 2 dB at all input voltage levels. The front end filter response was designed to have good passband attenuation and delay characteristics at the ex-

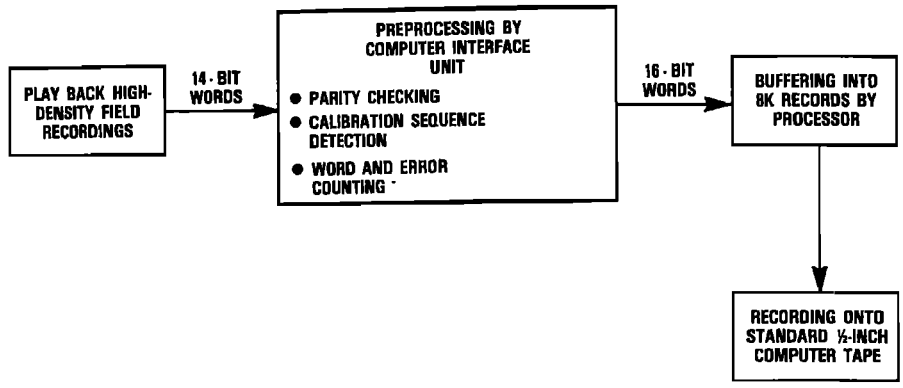

Fig. 4. Functional diagram of transcription process.

pense of gradual side lobe reduction. Subsequent digital filtering was used to suppress side lobe response steeply, when needed.

3. DATA TRANSCRIPTION SYSTEM

The function of the data transcription system is to convert the 14-track high-density noise recordings made in the field into standard, computer-compatible nine-track magnetic tape recordings. Figure 4 is a functional block diagram of the transcription process. During transcription, two additional bits were added to each 14-bit word from the high-density recording. The first bit was a parity error indicator, and the second bit indicated whether the data was noise or the calibration sequence. The resulting 16-bit words were transmitted to the processor which buffered and recorded them in 8192-word (8K-word) records on standard half-inch magnetic computer tape.

One standard half-inch computer tape 2400 feet in length can accommodate 2500 8K-word records recorded at 1600 bits per inch, or 20,480,000 16-bit words. Since the noise from each antenna is sampled 510,000 times per second, this amount of data corresponds to 40.2 s of noise recorded from a single antenna or to 20.1 s of noise recorded simultaneously from two antennas. Therefore a standard data run of 5 minutes of recording from two antennas, either sequentially or simultaneously, fills 15 standard computer tapes. Hence an essential feature of the transcription systems is the ability to transcribe continuously onto multiple magnetic tapes. This requires the use of two computer tape drives and software to switch automatically between drives after 2500 records have been written on each tape.

The transcription system used to process most of the measured data is shown in Figure 5. This system is based on a VAX 11/780 computer system equipped with three 120 inches/s, 1600 bits/inch tape drives. These tape drives permit the transcription process to occur at a data rate of 64×10^3 words/s. In order to accommodate program execution a 16-word buffer is included in the computer interface unit, and a special device driver is supplied for the DR11-B interface unit. This transcription system permits simultaneous field recordings made at 120 inches/s to be played

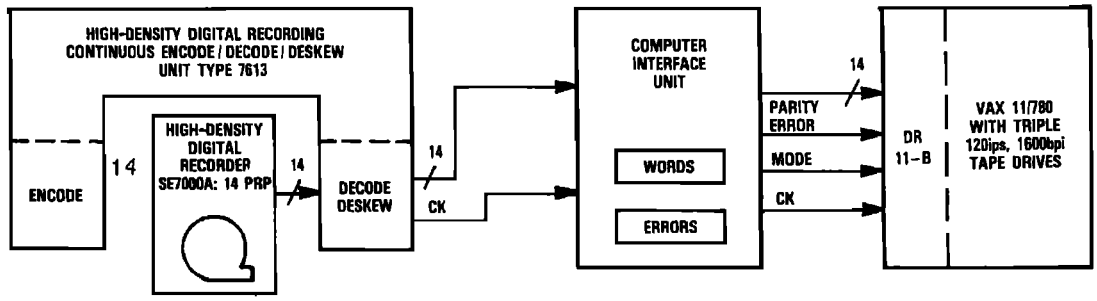

Fig. 5. Block diagram of transcription system.

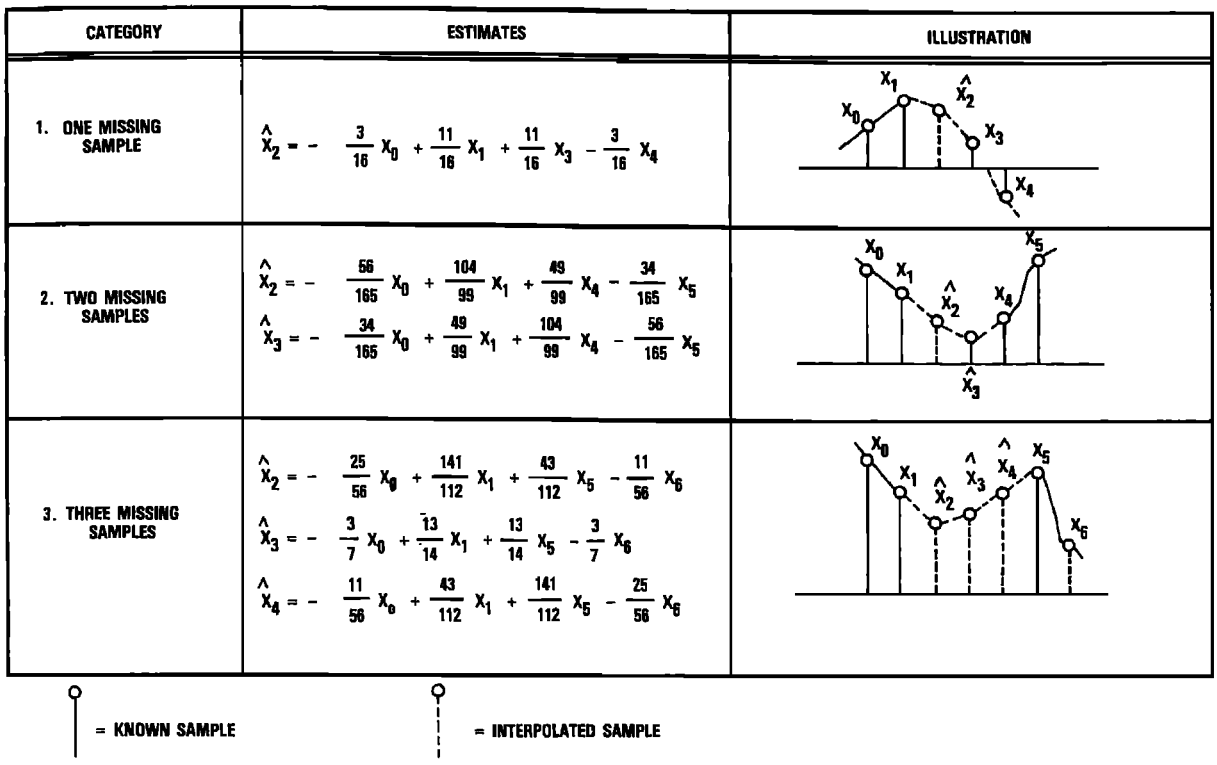

Fig. 6. Spline interpolation equations.

back at 7.5 inches/s resulting in a speed reduction ratio of 16 and acceptable error rates.

3.1. *Data reduction*

The data reduction process includes error control and data analysis. The error control function overcomes system errors during the transfer of data from computer magnetic tape to the computer disk storage. The sources of error include the high-density field tape errors and the computer magnetic tape errors.

Computer magnetic tape errors occur because the write, read, and check function normally performed in computer magnetic tape drives has to be disabled in real-time transcription. This procedure is followed to preclude data loss from the continuously running high-density tape recorder. The result is that when a block of data is written onto a bad section of tape and cannot be retrieved, a whole block is lost. In practice, most 2500-block tapes have no bad reads. In one check of performance on 100 tapes, four tapes had a total of five bad reads, for a block error rate of 0.002% from this source.

The high-density field tape errors are monitored via a parity bit that is carried as the fourteenth bit of each data word. With a single parity check on each word it is assumed that the individual channel error rate is so low that the probability of simultaneous errors on two channels is negligible. For cases where double errors occur the result is observable as an anomalous analysis result, which is discarded at that point. In practice, playback word error rates ranged from 10^{-5} to 7×10^{-3}. The error rate for the single-antenna data was nominally 4×10^{-4}, and for simultaneous data with a greater speed reduction factor the typical rate was 4×10^{-3}. Of course, the individual channel error rates average 14 times better. During transcription a hardware parity error test is performed on each word coming from the field tape replay system. A tape-to-disk program performs the primary error control function by either correcting errors or skipping data blocks in error.

3.2. *Error correction*

Error correction of bit errors involves use of four relationships that are inherent in the data samples

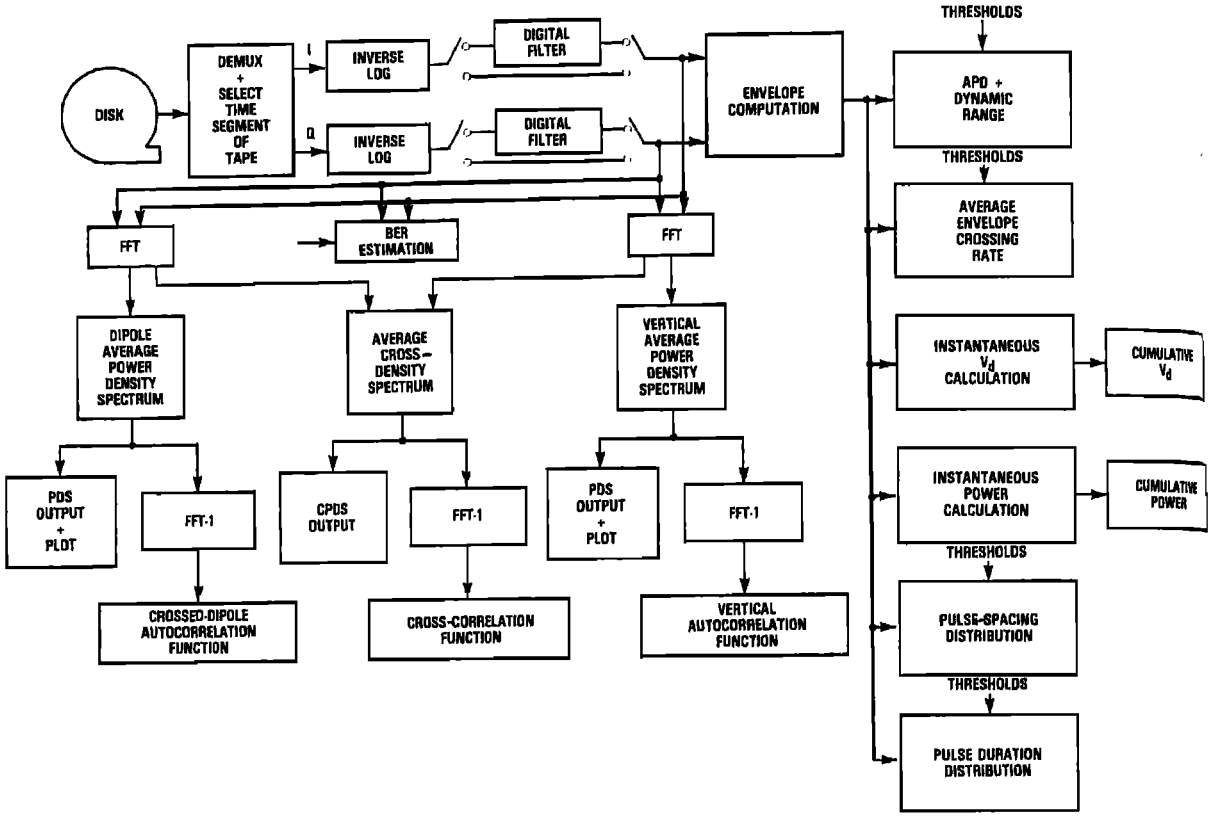

Fig. 7. Data analysis software.

and in certain aspects of the playback hardware. The fact that the data is oversampled by a factor of 2.5 times the Nyquist rate is the first factor utilized. Because the samples are dependent over a small interval, missing samples can be interpolated from neighboring ones. A spline method of interpolation is used by means of the equations shown in Figure 6. Three equations are provided to replace samples with various parity errors. These equations apply to one, two, or three noise sample losses. Each interpolation equation requires four correct noise samples as input: two samples immediately prior to the loss and two immediately following the loss. The inphase and quadrature channels are each interpolated independently. The same independent interpolation applies for simultaneous data from two antenna sources. The result is that for single-source data, up to six consecutive samples can be successfully recovered provided that four good samples precede and follow the error burst. For simultaneous data, up to 12 consecutive samples can be interpolated with eight good samples preceding and following the error burst. Since error bursts are primarily single and double errors, spline interpolation thus corrects the vast majority of error bursts due to the finite signal-to-noise ratio of the individual recorder channels.

The second and third relationships utilized in error correction are associated with recorder transmission characteristics. In order to transmit the 14 data bits in a parallel manner over 14 recorder channels, a technique for overcoming the deleterious effects of tape skew must be used. The function of the high-density digital recorder (HDDR) is to simultaneously insert on each channel a special block marker code between each 256 bits of data upon recording. During playback the HDDR recognizes the block markers, realigns the data into correct word groups, removes the block markers, and clocks data out at the appropriate rate. To the outside observer the block markers and the 256-bit block size are completely transparent so long as no HDDR-processing errors occur. Failure to correctly realign the data streams for one block results in an error burst of about 256-word duration. The algorithm for correcting skew errors uses test sequences of words in the error burst by examining advanced and retarded se-

quences for parity error. A second error correction algorithm based on delay modulation and known data is used to convert the actual sequence of bits from a given channel into a sequence of corrected data.

Finally, if the error sequence is too long for spline corrections and the skew or modulation rule tests have not proved successful, a variance technique is utilized. This technique is based upon the fact that the variance of the sum of two random variables is always greater than the variance of either variable. This last algorithm uses 13 trial sequences and selects the sequence with the minimum variance as the correct data. The use of the above four algorithms results in all data with correctable errors being transferred to the computer disk in contiguous blocks.

4. SOFTWARE DEVELOPMENT AND DATA ANALYSIS

The analysis software computes the following statistics and parameters: (1) voltage deviation (V_d), (2) amplitude probability distribution (APD), (3) noise power level (and by calibration F_a, as discussed in section 5.2), (4) power density spectrum (PDS), (5) cross-power density spectrum (CPDS), (6) autocorrelation function (ACF), (7) cross-correlation function (CCF), (8) pulse duration distribution (PDD), (9) pulse-spacing distribution (PSD), (10) average envelope crossing rate (ACR), (11) dynamic range, and (12) bit error rate (BER) receiver estimation. An overview of the data analysis software is shown in Figure 7. The software was developed to run on either a DEC 20-60 or a VAX 11/780 computer. Benchmark times of 0.5 and 1.5 s per 8192-word block for analysis of APD, V_d, and power calculations alone and with power density spectrum, respectively, have been obtained on the DEC 20. A computer run for 5 s of noise takes about 1 hour and 20 min of central processor unit (CPU) time.

The cross-power density spectrum (CPDS) and cross-correlation functions (CCF) can be computed because simultaneous measurements of both antennas were made in the winter and summer measurement periods. The software calculates fast Fourier transforms (FFT's) of vertical whip and crossed-dipole data on a block-by-block basis and forms the cross-density spectrum by multiplying one spectrum by the complex conjugate of the other and averaging the product over the duration of the measurement. The inverse FFT results in the cross-correlation function (CCF).

An executive program has been developed for the entire noise measurement data analysis project. This program can accept several different types of data and can analyze data from all three measurement periods including (1) sequential data (autumn and summer measurement periods), (2) simultaneous vertical and horizontal data (winter and summer measurement period), (3) simultaneous normal and quadrature output data, and (4) simultaneous data selected with the following options: length of data to be analyzed, data accumulation and printout interval, band-pass filtering or no filtering, FFT block length, averaging and printout interval, and specific data analysis statistics.

The program reduces one block of data at a time. For each block the data are filtered, calculations are performed, and a check is done to verify that the specified length of data has been read correctly.

4.1. *Data processing operations*

The processing of the noise recordings consists of two distinct phases, i.e., the survey processing and the detailed processing. Each phase in turn consists of two separate operations, transcription and analysis. This two-phase procedure is necessary because of the large amount of computer time required for the detailed analysis of each recording. A typical detailed analysis of 30 s of noise from each antenna with all program features implemented would require 14 hours of CPU time, whereas a typical survey analysis of 5 s of noise from each antenna would require only 1 hour of CPU time. In this way it is possible to sample the characteristics of all the noise recordings with the survey processing and conserve CPU time during detailed analysis by analyzing only one set of typical recordings in addition to those recordings which bracket the observed range of statistics.

4.2. *Survey processing*

Survey processing consists of the transcription and analysis of short segments of noise from each of the noise recordings made during each measurement period. Its primary purposes are (1) to obtain first-order statistics from all the available noise recordings, and (2) to serve as a basis for selecting a limited number of noise tapes for the more time-consuming detailed processing.

For the autumn measurement period during which sequential recordings from the two antennas were made, the survey transcription of each of the 149 noise recordings produced two computer tapes, one

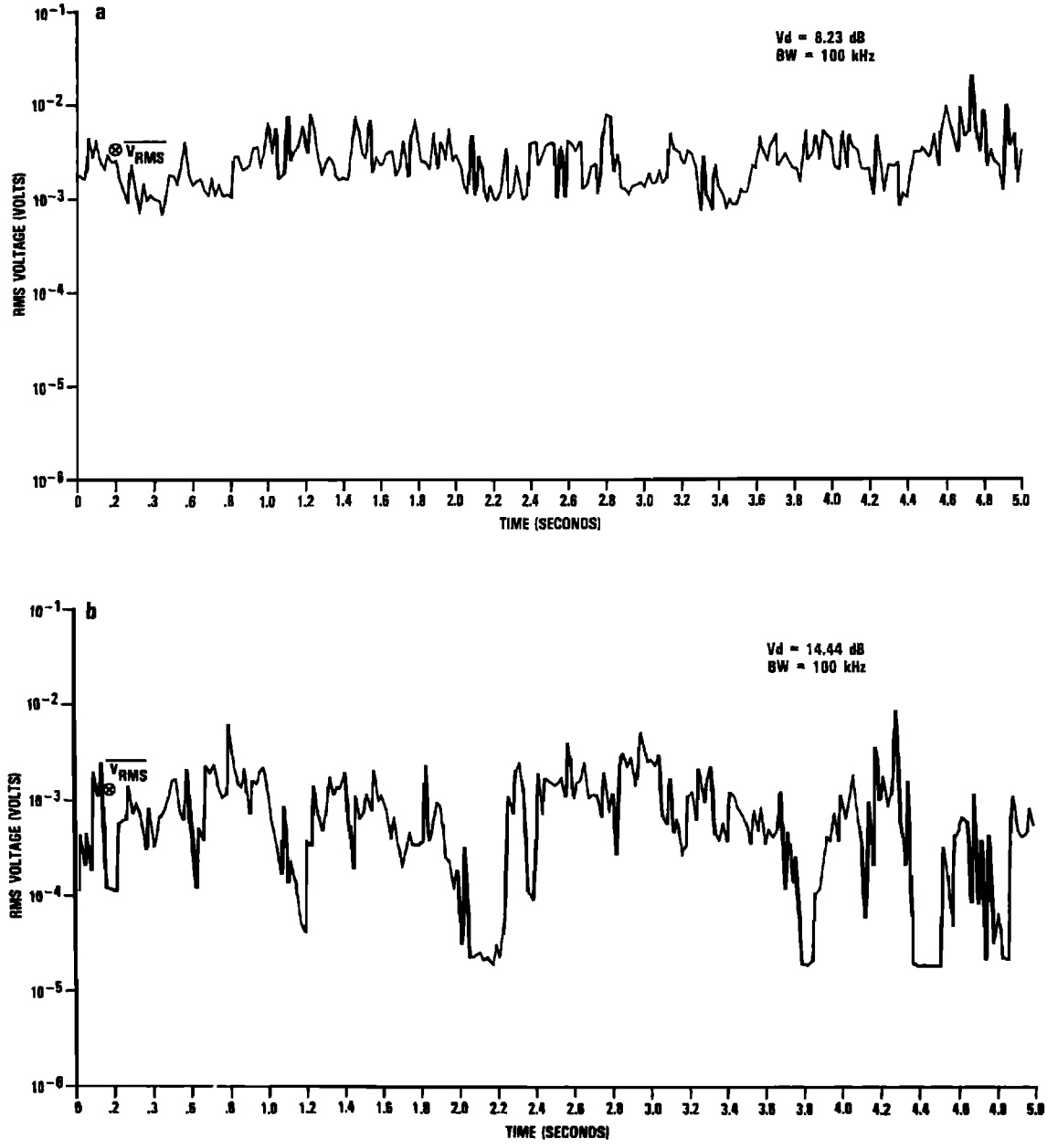

Fig. 8. Temporal structure of 450-kHz atmospheric radio noise for various levels of V_d. Five-second samples averaged every 20 ms. (Note change of bandwidth in Figure 8*d*.)

containing 40 s of noise from the vertical whip antenna and one containing 40 s of noise from the crossed-dipole antenna. The survey analysis of the autumn data was based on calculations of F_a, V_d, APD, PDS, and ACF, using 10–30 s of noise from each computer tape.

For the winter measurement period during which simultaneous recordings were made from the vertical whip and crossed-dipole antennas, the survey transcription of each of the 186 noise recordings produced one computer tape containing 20 s of noise from each antenna. Five seconds of simultaneously recorded noise from this tape were then filtered and analyzed, providing calculations of F_a, V_d, APD,

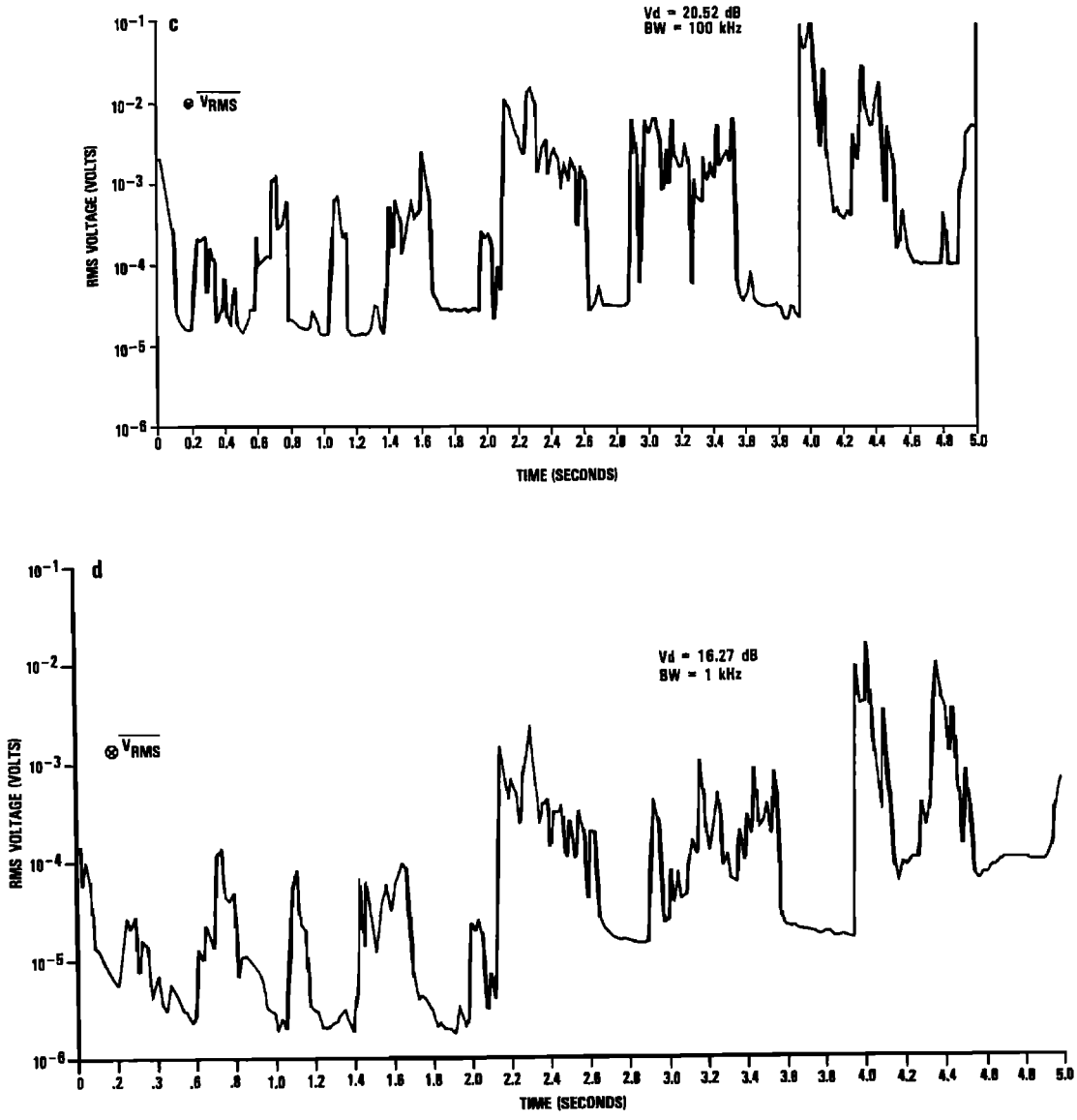

Fig. 8. (continued)

PDS, and ACF for each antenna and the CCF for both antennas.

For the summer measurement period the survey transcription produced two computer tapes from each of the 252 noise recordings. One tape contains 20 s of simultaneously recorded noise from the vertical whip and crossed-dipole antennas; the second tape contains 20 s of simultaneously recorded noise from the right-hand and left-hand circularly polarized outputs of the crossed-dipole antenna. From each of these tapes, 5 s of simultaneously recorded data was filtered and analyzed to obtain F_a, V_d, ADP, PDS, and ACF for each antenna and the CCF for both antennas.

4.3. *Detailed processing*

Detailed processing consisted of the transcription and analysis of long segments of noise from a selected subset of the noise recordings from each measurement period. All the statistical routines described above, including PDD, PSD, and ACF, were implemented during detailed analysis, and in some cases, additional special processing was performed. The

special processing includes repeated filtering of the same noise to different bandwidths to determine the effects of bandwidth on various parameters and the addition of simulated carriers to the noise to measure the change in V_d and other statistics as a function of carrier-to-noise ratio.

For the autumn measurement period, 50 recordings were selected for detailed analysis. The majority of these recordings were free of carriers, but several examples with carriers were deliberately included in the detailed processing to illustrate the effects of carriers on the statistics of the noise. The selected noise recordings included examples with high-, medium-, and low-V_d as well as high- and low-F_a values. The entire 5 min of noise recorded from each antenna was transcribed to magnetic computer tape. However, because of the amount of CPU time required to digitally filter the noise and to perform the pulse duration and pulse-spacing calculations, only 30 s of noise from the crossed-dipole antenna was submitted for detailed analysis. No detailed analysis of the noise from the vertical whip was performed, since the survey analysis had shown that noise from the two antennas was not significantly different.

For the winter measurement period, only recordings which were carrier free, or which could be made carrier free by filtering and still have bandwidths in excess of 25 kHz, were considered for detailed processing. Only 20 such recordings were identified. Forty seconds of simultaneously recorded noise from the two antennas were transcribed onto computer tape, and detailed analysis was performed on 30 s of the noise. For the summer measurement period the detailed processing consisted primarily of special analysis of eight carrier-free recordings to determine bandwidth effects on V_d and other parameters. Results of the detailed analysis are described in part 2 of this paper [*Giordano et al.*, this issue].

5. MEASURED NOISE CHARACTERISTICS

Operation of the noise measurement system as described in section 2 yielded a unique and extensive wideband, MF atmospheric radio noise data base, which has been partially analyzed using the computer software outlined in section 4. The survey analysis results for average noise power are presented and discussed in this section. Data from both the short vertical dipole antenna and the buried, horizontal, crossed dipole array antenna were utilized. In addition, wideband (100 kHz) data from the ANR and manually logged narrow band (10 kHz) data from the APD monitor were used.

The generally good agreement found between the various types of measurements speaks well of the integrity and reliability of the data base. There are departures, of course, but the observed differences are usually explainable in terms of interfering signals in the wideband vis a vis the narrow band data, local storm activity, noise polarization effects, or nonsimultaneity of measurements. (In the present context, "local activity" means thunderstorms active within a radius of about 300 miles.) In the latter case it is useful to note that the APD monitor measurements were normally made immediately prior to each recording session, principally to determine dynamic range and average power level in order to select gain settings for the ANR. This time difference of a few minutes (never more than about 10 min) could contribute some difference, especially during periods of local thunderstorm activity. Before addressing the derived noise power variations, it is of interest to examine the temporal structure of the atmospheric noise as recorded on the digital tape.

5.1. *Temporal structure of MF atmospheric noise*

Little information exists on the time waveforms of MF wideband noise, even through it is within this portion of the spectrum that the character of atmospheric noise changes from the discrete, time-separated pulses observed at VLF to the nearly continuous pulses characteristic of HF noise [*Malan*, 1958]. Because the thrust of the present effort was to characterize statistically the noise for use in radio systems performance evaluation [*Spaulding*, 1982], rather than to investigate the physics of generation mechanisms [*Uman*, 1969; *Golde*, 1977; *Volland*, 1982], only scant attention could be paid to the recorded waveforms. However, scrutiny of a few short-period samples of the recorded noise may provide better insight into the temporal structure of wideband MF noise and its relation to the statistical parameters to be discussed in part 2.

The temporal structure of the recorded noise is dependent upon the distribution of ranges and directions to active thunderstorms, the propagation conditions along those paths to the source regions (for example, ionospheric absorption and dispersion, ground conductivity), and the characteristics of the lightning discharges (for example, channel length and orientation, electric current distribution) within those regions. Recording of the noise on a routine basis for the statistical analysis performed here did not allow

for isolation of specific waveforms attributable to a particular lightning stroke or to an identified thunderstorm area.

For example, since more than one thunderstorm may be within range of the receiver, overlapping waveforms from independent sources may easily occur. A single lightning flash consisting of several (four or five) strokes will radiate a train of pulses that may persist up to a few hundred milliseconds. Additionally, since MF lightning signals (sferics) from all but the closest thunderstorms propagate via ionospheric reflections, a single sferic may arrive over several ray paths, say, one-, two-, and three-hop reflections, resulting in three groups of pulses separated by times equivalent to the difference in propagation time over the three paths. Finally, the dispersive character of the ionosphere (which causes the lower frequencies to travel slower within the medium) tends to broaden the pulse waveform in the time domain.

As a result, the temporal structure of the noise is highly variable. Three arbitrarily selected 5-s noise samples from the summer measurement period are given in Figures 8*a*–8*c* to demonstrate this variability as a function of V_d. (Figure 8*d* will be discussed later.) Each data point in the 5-s segment is a 20-ms rms average of the recorded voltage. Also, the rms voltage for the total segment (V_{rms}) is indicated at the beginning of each plot. It is clear that the relatively infrequent, large-amplitude spikes contribute most to V_{rms} of a 5-s noise sample. In Figure 8*a* it can be seen that for noise with a fairly low V_d the peak-to-valley ratio is relatively small, and there are no extended periods of very low noise level such as are evident in Figure 8*c* for the high-V_d case. The medium-V_d sample (Figure 8*b*), not surprisingly, has segments reminiscent of both the low- and high-V_d cases.

For Figure 8*d* the same 5-s sample used for Figure 8*c* was passed through a 1-kHz digital filter. The time variation is similar but not identical to that for the 100-kHz BW case, and its rms voltage is about a factor of 10 lower due to the two-decade decrease in bandwidth. Also, the calculated V_d is 4.25 dB lower for the 1-kHz than for the 100-kHz result, indicating that V_d decreases by about 2 dB per decade of bandwidth shrinkage rather than by 10 dB, as predicted by *CCIR* [1964], which is based upon the method of *Spaulding et al.* [1962].

To describe the behavior of the noise process statistically in part 2, recourse is made to the APD, V_d, ACR, PSD, and PDD, as defined earlier. Note that V_d is a single-number description of the noise impulsiveness wherein a high V_d implies a large dynamic range with discrete pulses. These statistics have all been described before for narrow band receivers [e.g., *Spaulding*, 1982], but their characteristics in wideband receivers appropriate for spread spectrum use have received little attention heretofore.

5.2. *Distribution of average power*

For investigation of the average power variations, 5- to 30-s segments of each field-recorded digital tape were surveyed in order to obtain a reasonable statistical sampling. Thus for the autumn measurement period, data from a total of 298 magnetic tapes were utilized, while for the winter and summer periods, data from 186 and 504 magnetic tapes were used, respectively. The data were taken with both the ANR and the APD monitor, using both antennas.

In the measurements the rms field strength was obtained by applying the antenna effective height and transmission line loss to the rms voltage at the antenna terminals. Then the noise power P_n is computed from the relationship [*CCIR*, 1964]

$$F_a = 10 \log \frac{P_n}{kT_0 B}$$

where k is Boltzmann's constant, T_0 is 288 K, and B is the bandwidth in hertz. The noise power factor for a frequency f in kHz, assuming a short vertical monopole, is given by

$$F_a = E_n - 20 \log f - 10 \log B + 155.5$$

where E_n is the rms field strength in decibels above a microvolt per meter.

Cumulative distributions of F_a for each season and each antenna were computed from the APD monitor data (Figures 9*a*–9*d*) and again from ANR survey samples (Figures 10*a*–10*d*). The number of measurements M in each cumulative distribution is the same for each antenna for the APD monitor data (Figures 9*a*–9*d*) but is usually different for the wideband ANR distributions. The effects of a carrier on the noise statistics were examined by eliminating measurement data having significant carrier contribution.

For comparison, whole-day predictions were derived from *CCIR* [1964] data, assuming that F_{am} is lognormally distributed [*Foldés*, 1960; *Horner and Harwood*, 1956]. With this assumption it is permissible to average the F_a's in dB. Table 3 shows the construction of the daily average F_{am} (24-hour composite) and standard deviation σ for each season. In autumn, for example, *CCIR*'s [1964] Figure 23A for 1200–1600 hours in Nevada shows the 450-kHz noise

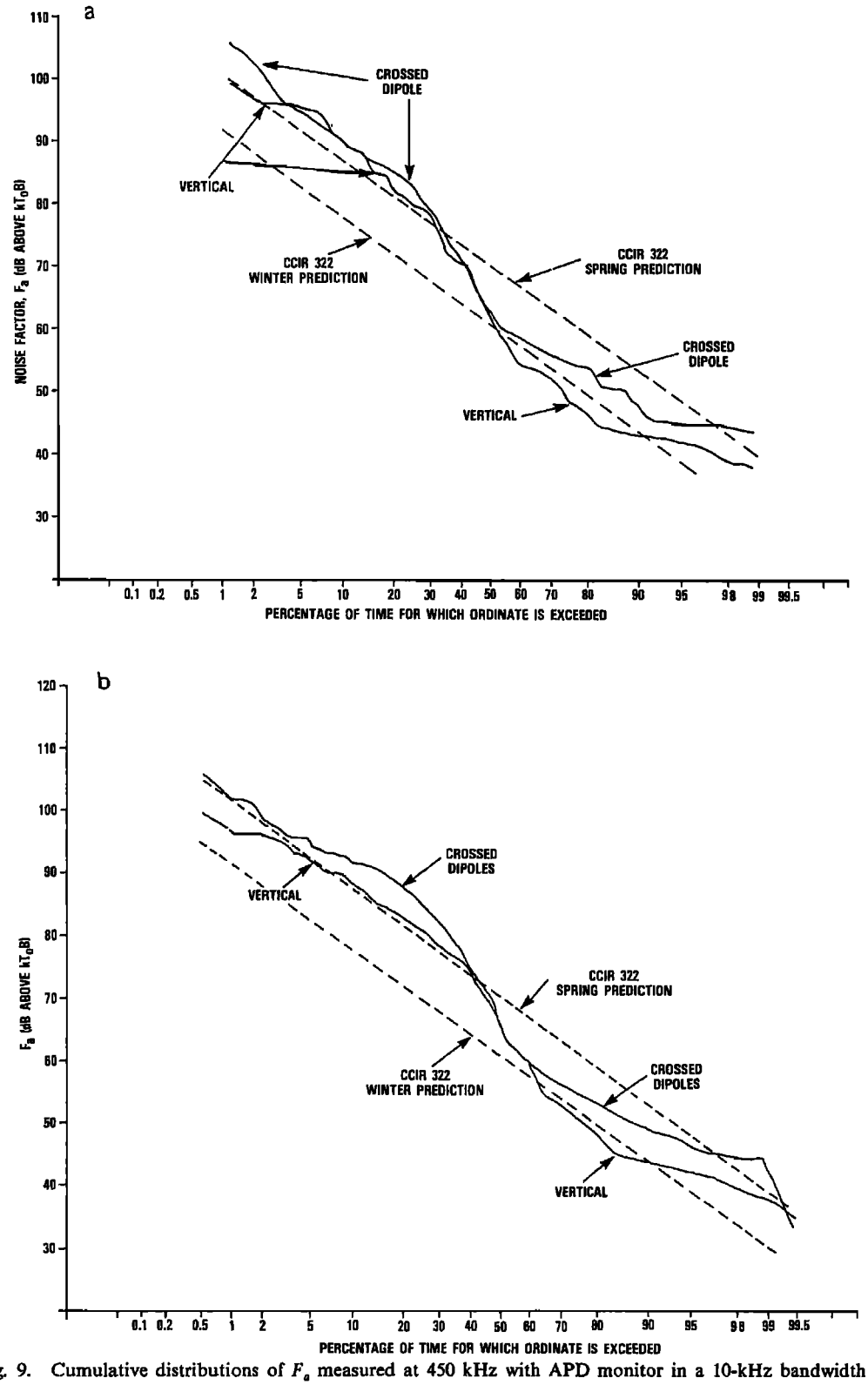

Fig. 9. Cumulative distributions of F_a measured at 450 kHz with APD monitor in a 10-kHz bandwidth: (*a*) winter data, carrier free; (*b*) all winter data; (*c*) autumn; (*d*) summer. (M is the number of noise samples used for each distribution, identical for each antenna.)

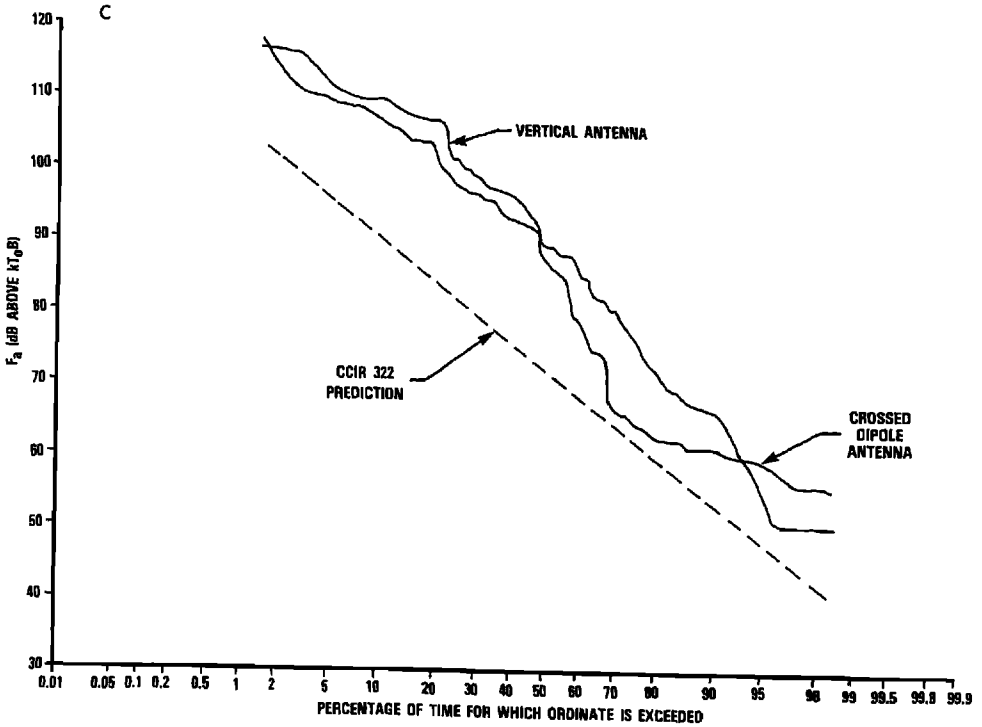

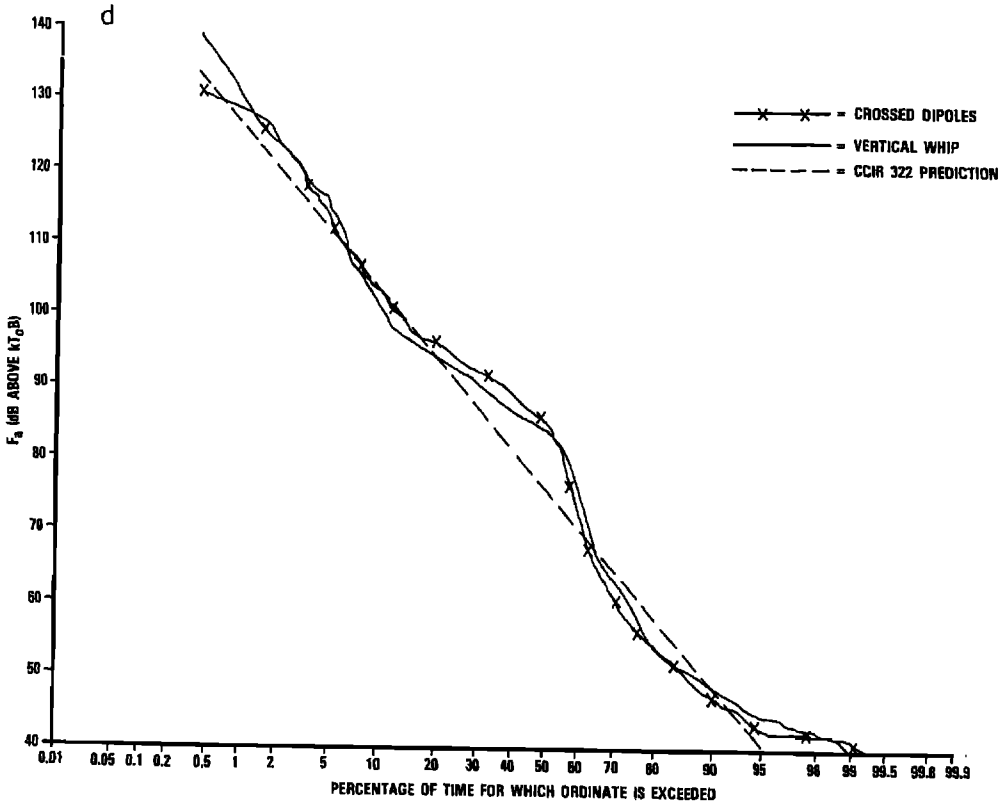

Fig. 9. (continued)

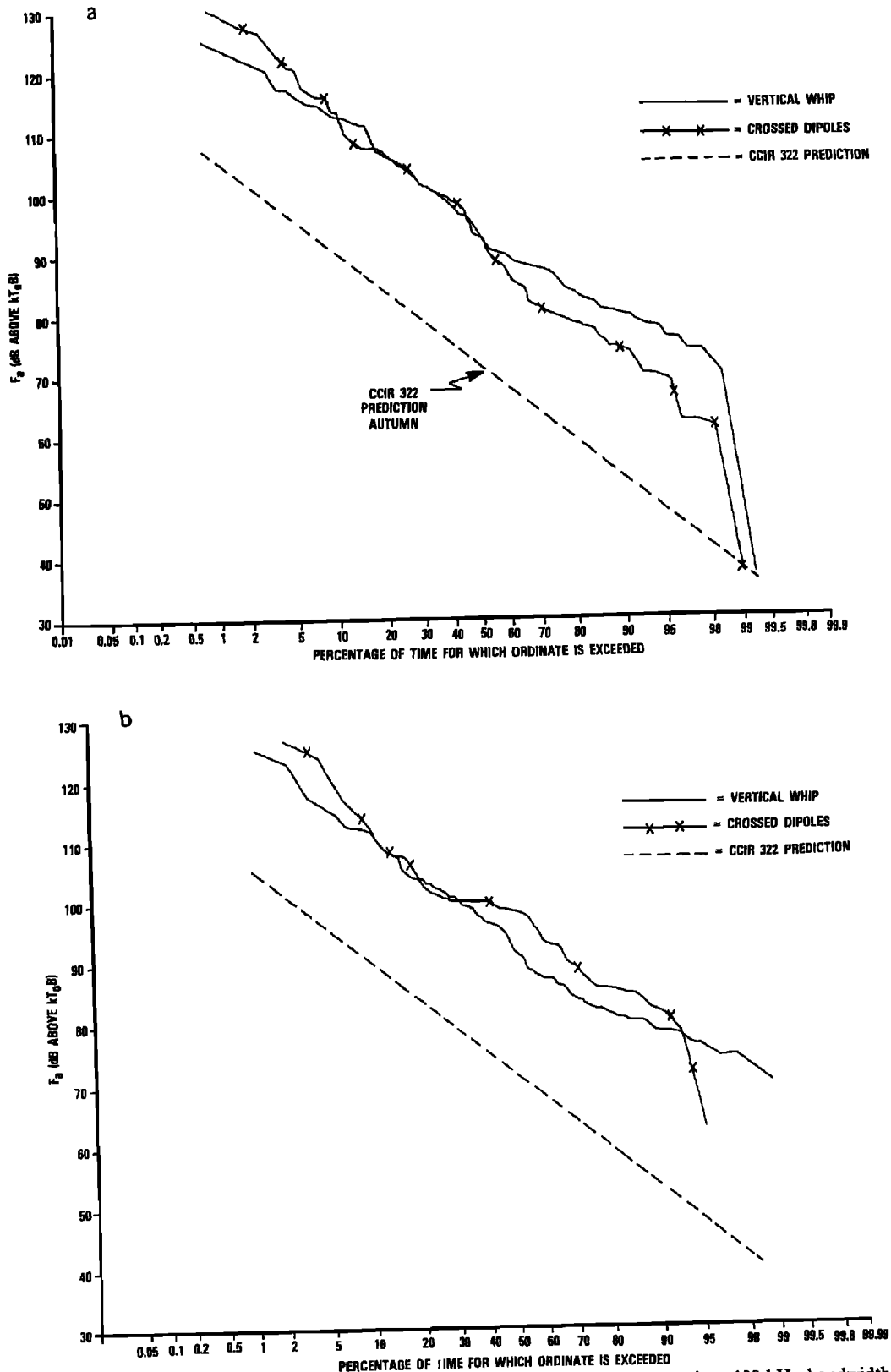

Fig. 10. Cumulative distributions of F_a measured at 450 kHz with ANR system in a 100-kHz bandwidth: (*a*) autumn data; (*b*) autumn data, carrier free; (*c*) summer data; (*d*) winter data. (M is the number of noise samples used for each distribution.)

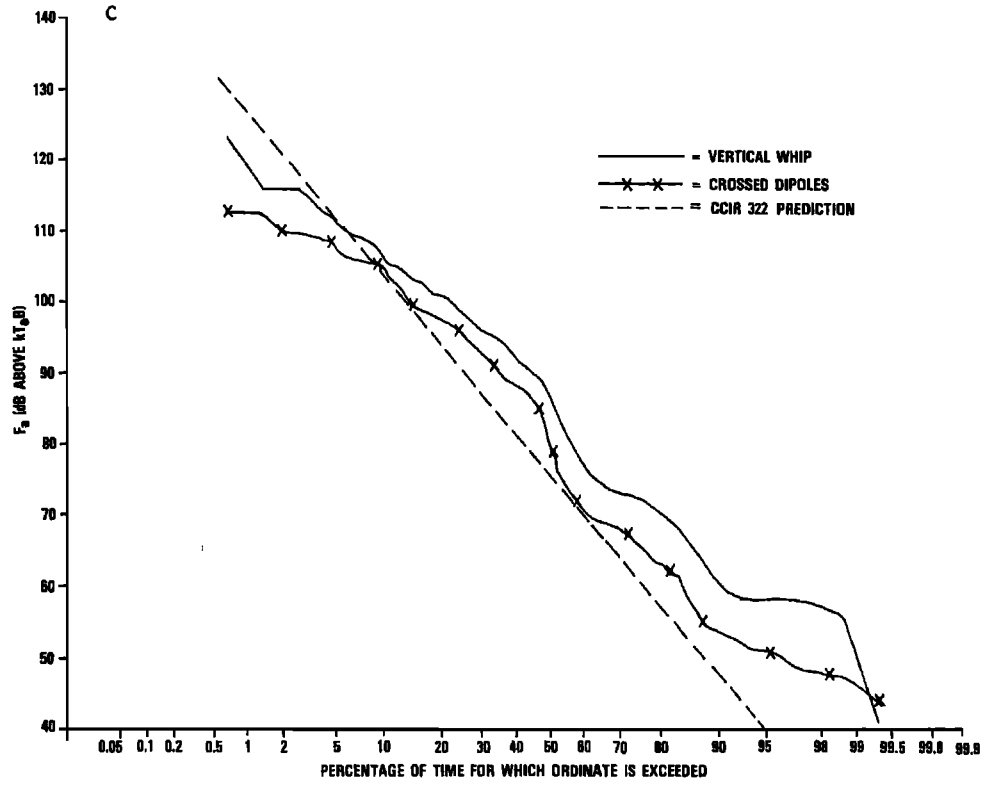

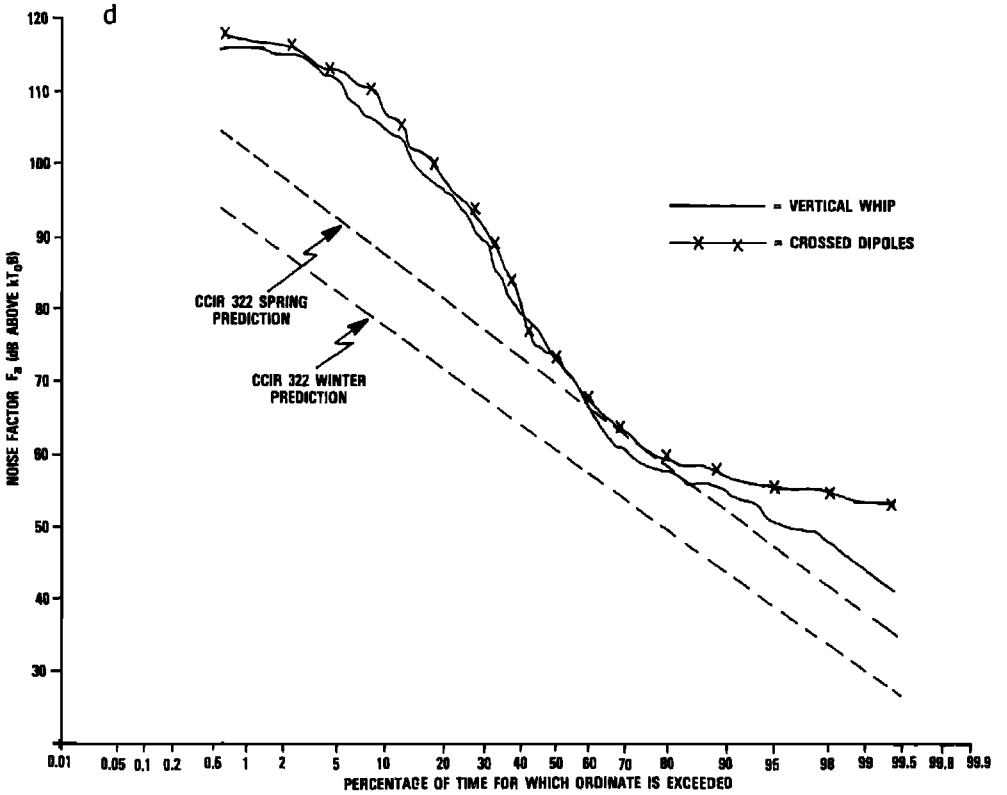

Fig. 10. (continued)

TABLE 3. Calculation of Cumulative Distributions From *CCIR* [1964] for F_a at 450 kHz

Time Block, hours	Autumn		Winter		Spring		Summer	
	F_{am}	σ	F_{am}	σ	F_{am}	σ	F_{am}	σ
0–400	88	4.6	73	5.1	84	4.0	84	5.8
400–800	71	5.3	69	4.7	65	5.7	70	7.9
800–1200	52	5.8	44	5.0	50	7.2	56	8.6
1200–1600	57	6.8	45	5.3	65	7.5	73	9.2
1600–2000	77	5.4	63	7.1	73	5.5	82	6.7
2000–2400	85	4.7	71	5.7	85	4.1	86	4.6
24-hour composite	71.7	14.5	60.8	13.2	70.3	13.4	75.2	12.7

level to be 57 dB, with a corresponding standard deviation of 6.8 dB, as given by *CCIR* [1964] Figure 11C. The 24-hour composite F_{am} is simply the average in decibels of the six CCIR time block values. The composite standard deviation, however, was computed by the formula

$$\sigma_c = \left[\frac{1}{6}\sum_{i=1}^{6}(\sigma_i^2 + (F_{ami} - F_{amc})^2)\right]^{1/2}$$

where i (=1 to 6) refers to each time block and F_{amc} is the 24-hour composite value of F_{am}.

The composite values for each season were used to construct the predicted [*CCIR*, 1964] cumulative distributions plotted as dashed lines in Figures 9*a*–9*d*. This was done by plotting F_{amc} at the 50% level and, to fix the slope, letting the value $F_{amc} + \sigma_c$ fall at the 16% level, which corresponds to one standard deviation from the median in a lognormal distribution. Note that because the "winter measurement period" was actually conducted in February and March, both winter and spring CCIR curves are used in Figures 9*a*, 9*b*, and 10*d*.

To facilitate comparisons the curves of Figures 9*a*–9*d* and Figures 10*a*–10*d* are summarized in Table 4. Here, a number of interesting features emerge. For example, in almost all cases the ANR (wideband) determination of median F_a is greater than that for the (narrow band) APD monitor by approximately 5–8 dB. Moreover, this holds true for both antennas except for the summer crossed-dipole measurement. The discrepancy is conjectured to result from the presence of carriers in the wider band measurement system.

For a final comparison of F_a measured with different equipment systems, cross correlations were calculated between the vertical whip and crossed-dipole antenna ANR measurements for autumn, winter, and summer. The highest cross-correlation coefficient (0.975) was found for summer, and the scatter is quite small (see Figure 11*a*). Similar data for autumn and winter (not shown) reveal a somewhat larger scatter of the data points with cross-correlation coefficients that are still quite high, that is, 0.84 and 0.97, respectively. It should be noted that in the winter and summer cases, measurements were made simultaneously with the two antennas, whereas the autumn measurements were made at different times on the two antennas. As a result, it is not surprising that the cross-correlation coefficient (0.84) is smaller for autumn than for the other two measurement periods.

Comparison of the autumn F_a determined with the ANR wideband system with those from the APD monitor (Figure 11*b*), again discloses the probable influence of interfering signals in or adjacent to the 100-kHz bandwidth. In Figure 11*b* it can be seen that the least squares fit of the data (solid line) has a smaller slope than the ideal curve represented by the

TABLE 4. Summary of 450-kHz F_a Distributions Measured by Different Techniques

Antenna Type	Source	Upper Decile	Median	Lower Decile	Number of Data Points
		Autumn			
Vertical	CCIR		71.7		
	APD monitor	110	89	66	69
	ANR survey	113	94	80	130
	ANR survey, carrier free	112	92	78	83
		Winter			
Vertical	CCIR, winter		60.8		
	CCIR, spring		70.3		
	APD monitor	88	66	43	183
	ANR survey	105	73	55	164
	ANR monitor, carrier free	90	62	43	83
Crossed-dipole	APD monitor	92	66	49	183
	ANR survey	108	74	57	164
	APD monitor, carrier free	90	63	47	83
		Summer			
Vertical	CCIR		75.2		
	APD monitor	101	84	49	246
	ANR survey	106	86	61	155
Crossed-dipole	APD monitor	103	85	47	246
	ANR survey	104	79	54	153

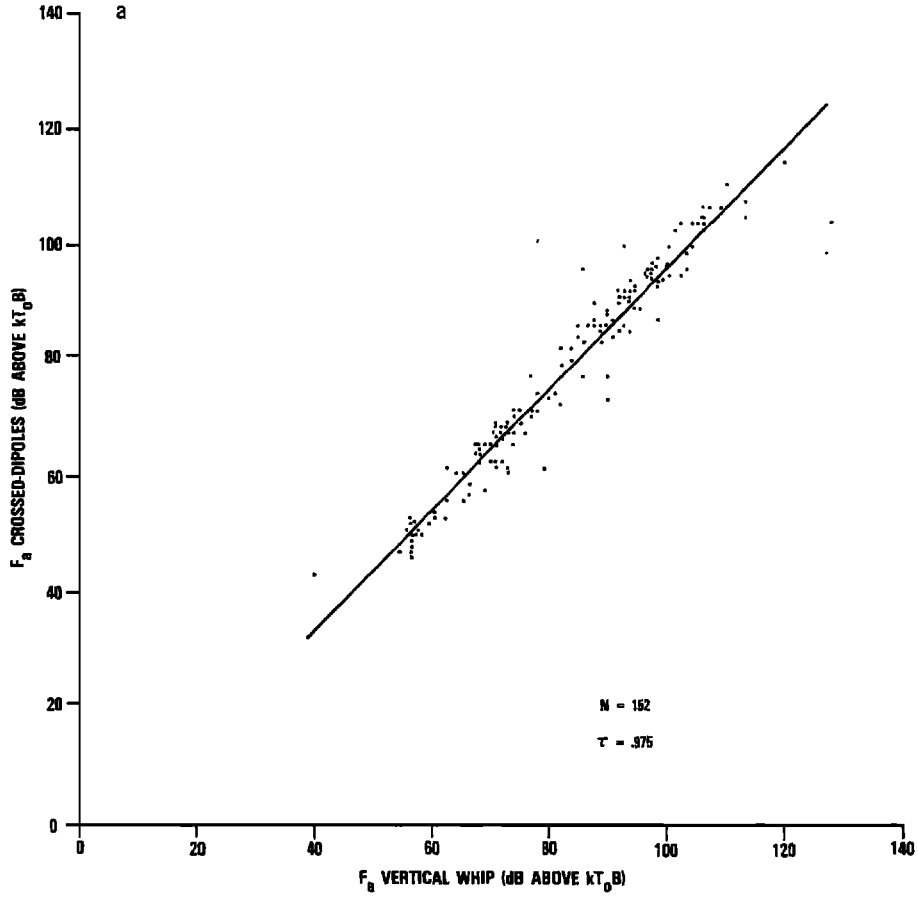

Fig. 11*a*. Cross-correlation scatter plots of F_a measured by ANR samples of vertical whip antenna against crossed-dipole antenna in summer period.

dashed line because the low values measured by the narrow band instrument are not matched by those from the wideband ANR. It is clear that interfering signals in the larger bandwidth, which are masked at the higher noise levels during the summer, begin to become more important as the ambient noise level drops.

In comparing the measured data with the predictions, it can be seen that in all autumn cases (Figures 9*c*, 10*a*, and 10*b*) the measured distributions are consistently higher than the CCIR curves by 10–20 dB. One explanation is that local thunderstorms were present on at least seven of the 29 days of ANR measurements and on at least four of the 15 days of APD monitor records. A second is that in lumping all taped samples together in the bulk survey processing, some samples containing interfering signals were probably included. In the other seasons, especially summer, the differences are not quite as great. The winter APD monitor data follows a distribution bounded by the CCIR winter and spring curves.

There is a clear seasonal variation in the data summarized in Table 4. Considering only the medians, it is evident that the lowest F_a was found in winter, consistent with expectations, and the summer values were much higher, also in accordance with CCIR predictions. The highest F_a values were observed in autumn. This departure may be explained by the frequent occurrence of local storm activity, which is not considered in the CCIR predictions.

The diurnal variations observed in the three measurement periods are illustrated in Figures 12*a*–12*c*. Separate curves are given for the APD monitor

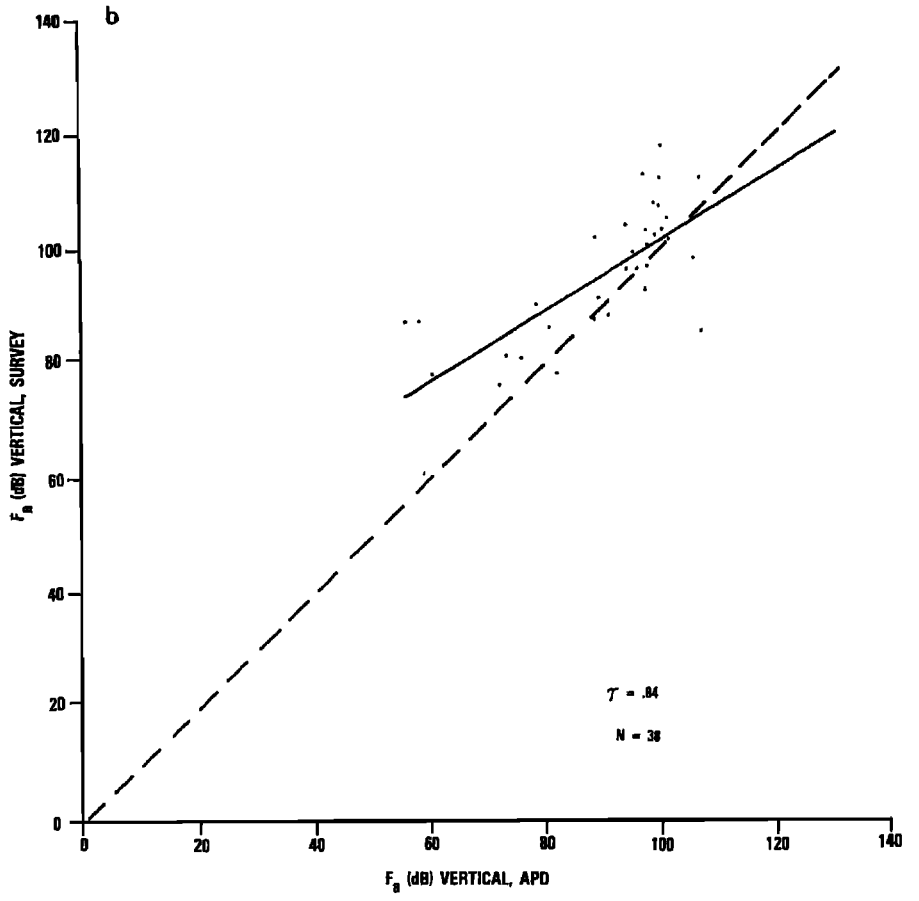

Fig. 11*b*. Cross-correlation scatter plots of F_a measured by APD monitor data against ANR data, both from vertical whip antenna in autumn period.

and ANR results. During summer (Figure 12*a*), the APD monitor variation is consistent with CCIR predictions, wherein F_a is low during the day and high at night. A similar pattern is seen in the wideband ANR results. In the latter case the daytime minimum remains larger than the results from either the APD monitor or CCIR. The unusual amount of thunderstorm activity occurring in the Nevada area in autumn 1980 is again apparent in the diurnal variations in Figure 12*b*. Both the ANR and APD monitor curves for 0800–1600 are much higher (~30 dB) than CCIR predicted, leading to a rather shallow diurnal curve. The winter measurement period (Figure 12*c*) also has the characteristic diurnal variation of MF noise, which results in high nighttime levels and low daytime levels.

6. CONCLUSIONS

In part 1 of a two-part sequence, the noise measurement and data transcription system along with the data analysis software for determining noise statistics have been described. Comparisons of the average noise power factor with CCIR predictions have been made for season and time of day. Typically, the measured noise factor is higher than CCIR predictions. In autumn, for example, the measured noise figure exceeded CCIR predictions by 10–20 dB, probably in part due to the presence of local thunderstorms. In part 2, further noise statistics obtained from the wideband measurement, transcription, and analysis system described here, as well as the impact of the noise environment on system performance, will be presented.

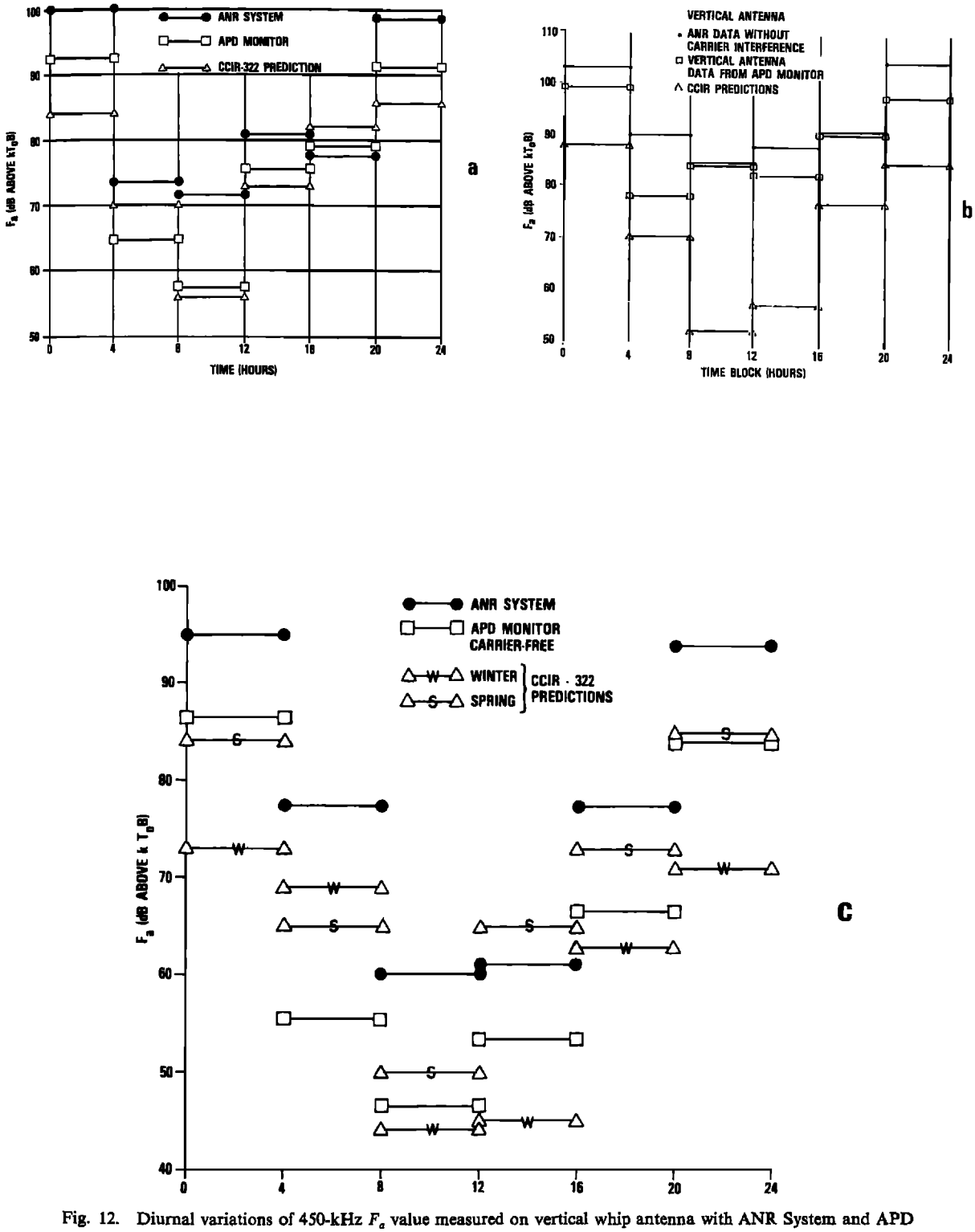

Fig. 12. Diurnal variations of 450-kHz F_a value measured on vertical whip antenna with ANR System and APD monitor, compared to *CCIR* [1964] predictions: (*a*) summer 1981; (*b*) autumn 1980; and (*c*) winter 1981.

Acknowledgments. The work reported here was supported by the Air Force Ballistic Missile Organization under contract F04704-79-C-0070. We acknowledge with thanks the long, grueling hours expended by M. Brooks and Tom White in the data processing effort and the many helpful discussions with H. Sunkenberg. We are indebted to Jack Ryan of the GTE Engineering Support Service for all of the field support required to carry out the experimental measurements in the remoteness of Nevada desert country.

REFERENCES

Foldés, G., The log normal distribution and its application to atmospheric studies, in *Statistical Methods in Radio Wave Propagation*, edited by W. C. Hoffman, pp. 227–232, Pergamon, New York, 1960.

Giordano, A. A., J. R. Herman, X. A. DeAngelis, K. F. Marzotto, and F. M. Hsu, Measurement and statistical analysis of wideband MF atmospheric radio noise, 2, Impact of data on bandwidth and system performance, *Rad. Sci.*, this issue.

Golde, R. H. (Ed.), *Lightning*, vol. 1, Academic, Orlando, Fla., 1977.

Herman, J. R., X. A. DeAngelis, A. A. Giordano, K. F. Marzotto, and F. M. Hsu, Considerations of atmospheric noise effects on wideband MF communications, *IEEE Commun. Mag.*, Nov., 24–29, 1983.

Horner, F., and J. Harwood, An investigation of atmospheric noise at very low frequencies, *Proc. Inst. Electr. Eng., Part B*, 743–751, 1956.

International Radio Consultative Committee, CCIR world distribution and characteristics of atmospheric radio noise, *CCIR Rep. 332*, Int. Telecommun. Union, Geneva, Switzerland, 1964.

International Radio Consultative Committee, Operating noise—threshold of a radio receiving system, *CCIR Rep. 413*, Int. Telecommun. Union, Geneva, Switzerland, 1966.

Malan, D. J., Radiation from lightning discharges and its relation to the discharge process, in *Recent Advances in Atmospheric Electricity*, edited by L. G. Smith, pp. 557–563, Pergamon, New York, 1958.

Marzotto, K. F., X. A. DeAngelis, J. R. Herman, and A. A. Giordano, Wideband measurements of medium frequency atmospheric radio noise, paper presented at IEEE Electromagnetic Compatability Symposium, Inst. of Electr. and Electron. Eng., Santa Clara, Calif., Sept. 8–10, 1982.

Spaulding, A. D., Atmospheric noise and its effects on telecommunications systems performance, in *Handbook of Atmospherics*, vol. 1, edited by H. Volland, pp. 289–328, CRC Press, Boca Raton, Fla., 1982.

Spaulding, A. D., C. J. Roubique, and W. Q. Crichlow, Conversion of the amplitude probability distribution function for atmospheric radio noise from one bandwidth to another, *J. Res. Nat. Bur. Stand., Sect. D*, *66*, 713–720, 1962.

Sunkenberg, H. A., A. A. Giordano, X. A. DeAngelis, and K. F. Marzotto, Measurements of wideband atmospheric noise, paper presented at IEEE International Conference on Communications, Inst. of Electr. and Electron. Eng., Seattle, Wash., June 8–12, 1980.

Uman, M. A., *Lightning*, McGraw-Hill, New York, 1969.

Volland, H. (Ed.), *Handbook of Atmospherics*, vol. 1 and 2, CRC Press, Boca Raton, Fla., 1982.

X. A. DeAngelis, and J. R. Herman, GTE Government Systems Corporation, Strategic Systems Division, 1 Research Drive, Westborough, MA 01581.

A. A. Giordano, CNR, Incorporated, 220 Reservoir Street, Needham, MA 02194.

F. M. Hsu and K. F. Marzotto, GTE Government Systems Corporation, Communication Systems Division, 77 "A" Street, Needham Heights, MA 02194.